Biomaterials Advances 176 (2025) 214359

Contents lists available at ScienceDirect

Biomaterials Advances

journal homepage: www.journals.elsevier.com/materials-science-and-engineering-c

Dynamic regulation of thermal-responsive fibers for mitomycin C-controlled delivery on glaucoma drainage device implantation

Jingyi Ma [a,1], Lu Wang [b,1], Aimeng Dong [a], Shiqi Zhang [a], Tao Guo [b], Yiling Han [a], Menglu Jiang [a], Pan Fan [a], Wulian Song [a], Fenghua Zhang [b,*], Jinsong Leng [b,*], Huiping Yuan [a,*]

[a] Department of Ophthalmology, The Future Medicine Laboratory, The Second Affiliated Hospital of Harbin Medical University, No. 246 Xuefu Road, Harbin 150086, People's Republic of China

[b] Centre for Composite Materials and Structures, Harbin Institute of Technology (HIT), No. 2 Yikuang Street, Harbin 150080, People's Republic of China

ARTICLE INFO

Keywords:
Controlled drug delivery
Ahmed glaucoma valve
Bleb Fibrosis
Mitomycin C
Thermal-responsive polymer fibers

ABSTRACT

Bleb fibrosis remains the most common reason for glaucoma surgery failure. Although mitomycin C (MMC) is often used to inhibit fibrosis during glaucoma drainage device (GDD) implantation, the effective reaction time of anti-fibrosis could not cover the dynamic process of wound healing. To enable noninvasive dynamic ocular drug release, we fabricated MMC-loaded thermos-responsive fiber membranes using polylactic acid (PLA) and tributyl citrate as a plasticizer. The fibers exhibited a transition temperature of 41.5 °C. To regulate drug delivery, the fiber was first stretched, coated on the GDD surface, and then implanted in rabbit eyes. The thermal-responsive fiber recovered to its original morphology upon exposure to a 43 °C stimulus in filtering bleb area one week postoperatively. The release profiles in vitro were described best by the first-order kinetics. The release rate constants were $k_{origin} = 0.11 \pm 0.01\ day^{-1}$ and $k_{stretched} = 0.09 \pm 0.02\ day^{-1}$, respectively. The controlled release system effectively reduced the bleb fibrosis in rabbit conjunctiva. This MMC-controlled delivery system successfully inhibited scarring after GDD implantation surgery.

1. Introduction

Glaucoma is an important cause of irreversible blindness [1], and surgery has remained the main treatment method for glaucoma. A glaucoma drainage device (GDD), such as the Ahmed glaucoma valve (AGV), is a valuable tool available for glaucoma surgical management. The AGV effectively reduces intraocular pressure (IOP) while treating primary, secondary, and refractory glaucoma [2]. Surgical success rates decrease over time, usually owing to fibrosis of the filtering bleb wall around the drainage device. The major determinant of surgical success is wound healing, and excessive wound healing causes subsequent bleb fibrosis and failure of surgery. Conjunctival wound healing is a cascade of dynamic events. After the phase of hemostasis and inflammation, fibroblasts proliferate massively and differentiate into myofibroblasts at the proliferative phase and reach a peak in the first postoperative week. The final remodeling phase shows excessive accumulation of extracellular matrix (ECM) components, including excessive proliferation of Collagen type I (Col1), and a dense subconjunctival scar forms finally [3]. Antimitotic such as mitomycin C (MMC) and 5-fluorouracil have been used to inhibit fibroblastic proliferation [4]. The common recommendations for the dose of MMC in AGV implantation is (0.2-0.5 mg/ml, 2-5 min), followed by irrigation with balanced salt solution (BSS). However, there is insufficient evidence that one intraoperative dose of MMC can reduce IOP of glaucoma patients undergoing GDD surgery according to a Cochrane review [5]. A single duration of MMC is not sufficient to resist the proliferation of fibroblasts caused by AGV as a foreign body constant simulation. During the conjunctiva wound healing, a dose of 20 to 25 μg MMC subconjunctival injections administered during and one week after surgery have been suggested to increase the long-term surgical success rate [6,7]. However, there is a chance that MMC subconjunctival injection could cause complications, such as avascular filtering blebs, inflammation, or subconjunctival hemorrhage [8]. Therefore, research efforts have focused on improving the effectiveness of antiproliferation agents in AGV implantation and decrease its complications [9–11]. Research on drug delivery systems has extended the duration of drug retention in the conjunctiva, thereby minimizing

* Corresponding authors.
E-mail addresses: fhzhang_hit@163.com (F. Zhang), lengjs@hit.edu.cn (J. Leng), yuanhp2013@126.com (H. Yuan).
[1] These two authors contributed equally.

https://doi.org/10.1016/j.bioadv.2025.214359
Received 5 October 2024; Received in revised form 15 April 2025; Accepted 25 May 2025
Available online 29 May 2025

administrations, discomfort, and systemic side effects. However, the above approaches initially showed a high drug release rate that decreased after the early stage, and this burst release may not cover the dynamic process of wound healing to raise the surgery success rate [12]. To overcome this issue, we developed a controlled drug release system using thermal-responsive polymers.

Thermal-responsive polymers can change from a programmed temporary shape to their original shape in response to external heat stimuli [13,14]. Biological thermal-responsive polymers have been widely used in ophthalmic drug delivery [15–17], tissue engineering [18], wound closure [19], and other fields [20]. Combining thermal-responsive polymers with fibrous structures produced by electrospinning can endow the polymers with unique characteristics, such as a large specific surface area, high permeability, and porosity [21]. In this study, a long-term *in vivo* study was carried out to realize the control of electrospinning deformation by external stimulation and non-invasive controlling of drug release rate.

Most thermal-responsive materials applied in ophthalmology have a transition temperature below 32–35 °C [22]. Herein, we introduce an MMC-loaded thermal-responsive polylactic acid (PLA)/tributyl citrate (TBC) fiber with a transition temperature of 41.5 °C. Compared to poly (N-isopropyl acrylamide) (PNIPAM) (prone to burst release near body temperature) or Polyethylene glycol (PEG)-based systems (characterized by rapid degradation and high hydrophilicity), PLA/TBC integrates advantages such as biodegradability, low inflammatory risk, and a stretch-recovery controlled release mechanism. The MMC-PLA/TBC-coated AGV was implanted in the experimental group. The fibrous membrane was first stretched above its transition temperature, cooled, coated on the AGV, and then implanted into rabbit eyes. The surface of the filtering bleb was then soaked with saline above the transition temperature (43 °C) for 30 seconds and MMC released faster non-invasively one week postoperatively. The dynamic drug release in vivo was achieved by polymers' thermal-responsive performance. Consequently, the fibers reverted to their original shape, and the drug release rate increased and was maintained at a certain level, thereby inhibiting long-term scar formation (the research process is shown in Scheme 1).

2. Materials and methods

2.1. Materials

Polylactic acid was obtained from Natureworks LLC (USA). TBC (>98%) was obtained from Aladdin Reagents Ltd. Dichloromethane (Analytical Reagent) was supplied by Tianjin Fuyu Fine Chemical Co., Ltd (China). N,N-Dimethylformamide (DMF, ≥99.9%, molecular biology grade) was supplied by Tianjin Fengchuan Chemical Reagent Technology Co., Ltd (China). Phosphate-buffered saline (pH 7.4) was procured from Shanghai Aladdin Biochemical Technology Co., Ltd (China). Mitomycin C was bought from Shanghai Anhui Pharmaceutical Co., Ltd (China). Ahmed Glaucoma Valves (model FP8, Rancho Cucamonga, CA) were provided by New World Medical Inc.

2.2. Preparation of thermal-responsive PLA/TBC and drug-loaded fibrous membrane

TBC was added to the thermal-responsive PLA; the content of TBC was adjusted to 6, 10, and 14 wt%. The polymer (PLA and TBC) was dissolved in dichloromethane (DCM) to achieve a final polymer concentration of 18 wt% in the mixed solution. For drug loading, the solutions with 3 wt% MMC dissolved in DMF were drawn into PLA-14 wt% TBC/DCM solutions and stirred at 100 rpm for 48 h away from light. Electrostatic spinning (Beijing Fuma, China) was conducted at 1 mL/h, voltage of 14 kV, and receiving distance of 22 cm at 25 °C with a 23G spinning needle. Finally, the membranes were removed from the collector and dried at 25 °C in the dark for three days.

2.3. Characterization

Membranes were observed using scanning electron microscopy (SEM, SU5000, Hitachi, Japan). The diameter distribution and porosities were measured using the ImageJ software. The transition temperature was tested using Differential Scanning Calorimetry (DSC) (Mettler Toledo, Switzerland); the temperature ranged from 0 °C to 200 °C, and the heating rate was 10 °C/min. Thermal stability was tested by Thermogravimetric analysis (TGA) (Mettler Toledo, Switzerland); the

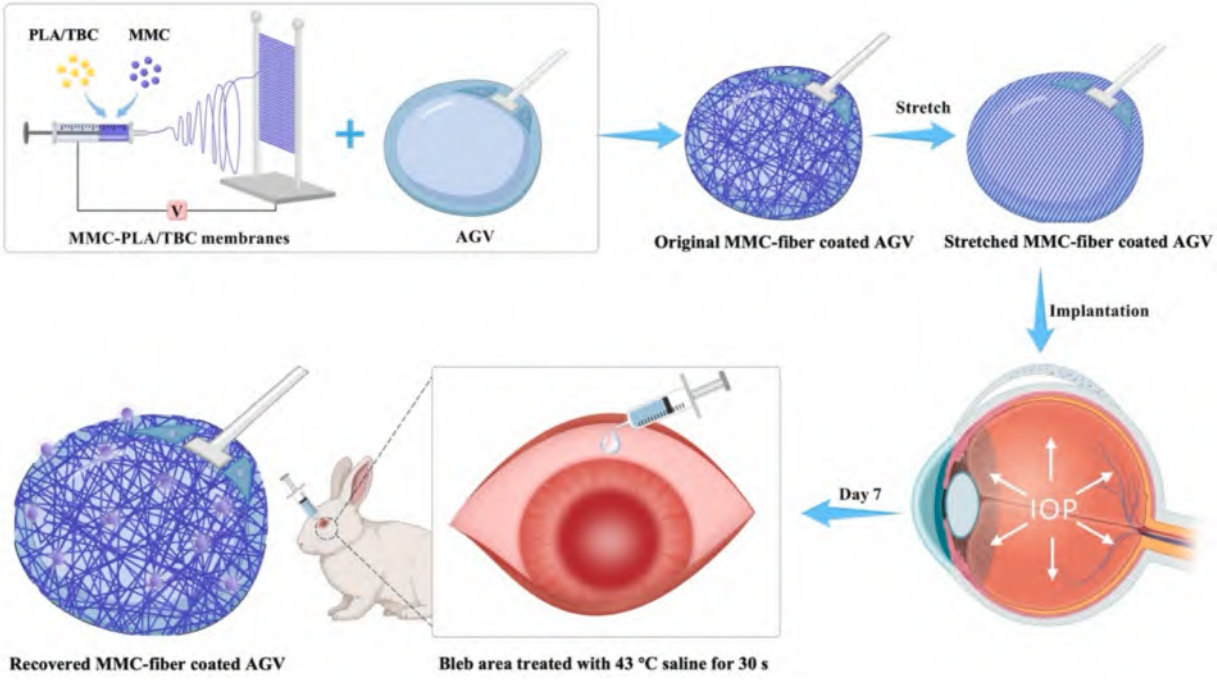

Scheme 1. Design of MMC-PLA/TBC-coated AGV and controlled drug release postoperatively. (This figure was created by the author.)

temperature ranged from 25 °C to 500 °C, and the heating rate was 10 °C/min. The infrared spectrogram was recorded using Fourier Transform Infrared Spectroscopy (FTIR). The water contact angle was tested using a contact angle measuring instrument (JY-82B, KRUSS, Germany). The degradation performance was tested in vitro and in vivo. Both PLA and PLA/TBC membranes were implanted into rabbit conjunctival sac, and the weight loss rate was calculated 7 and 14 days postoperatively. On day 14, conjunctival tissues around the membranes were stained by H&E.

2.4. Drug release study

The method reported by Dong et al. was used to evaluate the drug release properties of MMC-loaded thermal-responsive PLA/TBC membranes ensuring sink conditions were maintained for sustained MMC release [9]. A microinjection pump was used to simulate the humor flow of rabbit eyes. The study was performed in PBS medium (pH = 7.4) at 37 °C. A filter (450 mm^2) was connected to a 20-mL injector filled with PBS, and a size of 450 mm^2 MMC-loaded membrane was weighed and placed in the filter. The rates of MMC release were measured in original shape and stretched shape. In modified group, the fiber was stretched on first day and heated to 43 °C on day 7. The inject speed was 0.1 mL/h, and the MMC/PBS solution was collected every 24 h. The concentration was measured and calculated using a microplate reader at a wavelength of 364 nm (Biotek Synergy H1, USA). The release kinetics of MMC from both the original and stretched membranes were evaluated using zero-order, first-order, Higuchi, and Korsmeyer–Peppas models. Based on these kinetic analyses, the corresponding release rate constants (k) were determined. Furthermore, the diffusional exponent (n) derived from the Korsmeyer–Peppas model was also calculated to elucidate the underlying release mechanism.

2.5. In vitro cell culture

New Zealand white rabbits (supplied from Laboratory Animal Research Center, the second Affiliated Hospital of Harbin Medical University) were intravenously anesthetized with 3% pentobarbital sodium, and fresh Tenon's capsule tissue was collected from 3 healthy adult rabbits. Tissues were cut into fragments and adhered to the petri dish bottom. Primary Rabbit Tenon's Fibroblasts (RTFs) were obtained and passaged three to five times. Cells were incubated in Dulbecco's modified Eagle medium (DMEM) supplemented with 15% fetal bovine serum and 1% penicillin–streptomycin solution (5% CO_2, 37 °C).

2.6. Cytotoxicity and inhibitory effects of thermal-responsive PLA/TBC and MMC-loaded fibrous membrane

RFTs were seeded into a 24-well plate at 10^4 cells/cm^2 for 24 h. Micro/nano-fibrous membrane disks 15 mm in diameter were sterilized using 75% ethanol for 30 min. After repeated washes with PBS, membranes were subjected to UV irradiation at a wavelength of 254 nm in a cell culture hood for at least 30 min each side and treated membranes were folded and placed in Transwell inserts (6.5 mm diameter, 8-μm pore) with 300 μL of complete medium and 500 μL added to the lower compartment for subsequent experimental procedures. Membranes were divided into four groups: A (blank control), B (PLA/TBC membrane), C (MMC-PLA/TBC membrane), and D (stretched MMC-PLA/TBC membrane). Membranes in the Transwell chamber, On days 1, 5, and 7, the medium was replaced with 100 μL 10% cell counting kit-8 (Dojindo Laboratories, Kumamoto, Japan) DMEM solution for 30 min, and the medium absorbance was measured at 450 nm. Cell viability and inhibition of cell growth rate were calculated by comparison with those in the blank control group. Transwells and medium were removed on day 5, and 100 μL of live and dead staining reagent (Molecular Probes, Eugene, OR, USA) were added. Cell viability was assessed using fluorescence microscopy (Leica DM2500, Germany) after 30 min of incubation at 37 °C in the dark. Green fluorescence represents live cells and red fluorescence represents dead cells.

2.7. In vivo animal studies

2.7.1. Surgical section

Thirty female New Zealand white rabbits, weighing 2.0-2.5 kg were used in this study. Rabbits were divided into five groups: AGV control, PLA/TBC, MMC, MMC-PLA/TBC, and modified MMC-PLA/TBC (n = 6 animals per group). Specifically, in the MMC group, a cotton pad soaked with MMC solution (0.2 mg/mL) was placed in the conjunctival sac for 2 min and then thoroughly cleaned. In the PLA/TBC and MMC-PLA/TBC groups, the fibrous membrane was coated around the AGV surface and then implanted. In the modified MMC-PLA/TBC group, the fibrous membrane was heated to 43 °C, stretched, cooled, and coated around the AGV, and then implanted. The stretched fibrous membrane was recovered to the original form one week postoperatively. More specifically, the bleb area of rabbit's conjunctival sac was continuously exposed to 20 mL of 43 °C saline dripping and soaking for 30 seconds at room temperature.

A preoperative slit lamp, fundus examination, and baseline IOP were performed. Intraocular pressure was measured using a Tono-Pen AVIA Applanation Tonometer (Reichert Technologies, NY). Topical antibiotic drops were applied three days before surgery to reduce the postoperative inflammatory response. Rabbits were intravenously anesthetized using 3% pentobarbital sodium (1.2 mL/kg). Under surgical asepsis, the AGV was initialed before implantation. The Tenon's capsule was bluntly separated posteriorly. A 6-0 nylon suture fixed the drainage valve to the sclera 3.5 mm posterior to the corneal edge. The drainage tube was inserted 2–3 mm after a 23G needle punctured into the anterior chamber of the rabbit eye. Finally, the conjunctiva was continuously sutured. Postoperatively, anti-infective eye drops were used three times a day for two weeks. Postoperative intraocular infection, intraocular hemorrhage, accidental animal death, or exposure of the implant/drainage tube will be excluded.

2.7.2. Follow-up observations

The IOP and condition of the anterior segment of operation eyes were assessed postoperatively on days 1, 7, 30, 60, and 90. The thickness of the filtering bleb was measured using AS-OCT (Optovue, Fremont, CA, USA) on days 14, 30, 60, and 90. The fixing suture was identified as a marker line. Maximum and minimum thickness values were analyzed 3 mm posterior to the marker line.

2.7.3. Histology, immunohistochemistry, and immunofluorescence

Rabbits were euthanized by overdose anesthesia three months postoperatively. Bleb surrounding tissue (conjunctiva and sclera nearby) was carefully removed. Following paraffin embedding, tissue sections (5 μm thick) were prepared using a microtome and subsequently stained with hematoxylin and eosin (H&E) and Masson's trichrome for histological analysis; tissue was also immunostained for smooth muscle α-actin (α-SMA) (PTM-5671) and proliferating cell nuclear antigen (PCNA) (10205-2-AP). Images were acquired using an optical microscope (Leica DM IL LED, Germany). Tissue was immunostained for Col1 (14695-1-Ap) and Col3 (22734-1-AP), and then viewed under a fluorescence microscope.

2.8. Statistical analysis

Data are represented as mean ± standard deviation and analyzed with one-way analysis of variance or Student's t-test using the GraphPad Prism software 9.0. Results were considered significantly different if $P < 0.05$.

3. Results

3.1. Characterization of PLA/TBC micro/nano-fiber membranes

As shown in Fig. 1a, the DSC results suggest that the transition temperature of thermal-responsive PLA (65.6 °C) does not meet the requirements of biological applications and the temperature over 45 °C was indicated to be harmful to cells [23]. We therefore induced different contents of plasticizer TBC to decrease the transition temperature. As TBC content increased to 14 wt% of PLA (PT14), the transition temperature gradually decreased to 41.5 °C as shown in Fig. 1a. The thermogravimetric analysis (TGA) test presented in Fig. 1b shows that the PT14 fibrous membrane began to degrade at ~200 °C. The T5%, T95%, and Tmax (5%, 95%, and max weight loss temperature) values were 252 °C, 377 °C, and 383 °C, respectively, indicating good thermal stability of the PT14 fibrous membrane. Fig. 1c is the stress-strain curves of PLA, PLA/TBC, and MMC-PLA/TBC fiber membranes, which show that PLA fiber membranes have the largest breaking strength, the smallest elongation at break, and no obvious yield platform. TBC reduces the tensile strength of the fiber film and greatly improves the toughness. In addition, the addition of MMC increases the tensile strength of the fiber membrane and does not affect the toughening effect of TBC too much. To test the thermal-responsive performance, the PLA/TBC membrane was heated to 41.5 °C, stretched, cooled, and shape fixed. The fiber membrane recovered from the stretched shape in 10 s when soaked in 41.5 °C saline as shown in Fig. 1d. The thermal-responsive performance of PLA/TBC coated around the AGV was showed in Figure S1.

The degradation feature was tested in PBS buffer (37 °C, 120 rpm air bath shaker). PLA and PLA+14%TBC membranes are degradable, and PLA+14%TBC has faster degradation rate because of the small molecular weight of TBC (Fig. S2a). Fiber membranes were implanted in rabbits' conjunctival sac. Membranes were barely degraded in vivo within two weeks (Fig. S2b). Both membranes showed good biocompatibility in rabbits' eyes. A few inflammatory cells can be seen compared to the normal conjunctival tissues (Fig. S3).

3.2. Structure and drug release profiles for thermal-responsive fiber membranes

The morphology of the thermal-responsive PLA/TBC fiber membrane was observed using scanning electron microscopy (SEM) (Fig. 2a). The fibers were randomly oriented when arranged in their original shape, and the diameters of unloaded and drug-loaded fibers were 4.39 ± 1.49 and 2.13 ± 1.32 μm, respectively. When stretched, the fibers were aligned in the same orientation, and the diameters of unloaded and drug-loaded fibers were 3.67 ± 1.13 and 1.04 ± 0.29 μm, respectively. The diameter of the fibers after stretching was significantly smaller ($p < 0.001$) than those of the original structure in Fig. 2b. There was a significant difference ($p < 0.0001$) in porosity between the original and stretched drug-loaded fibers (11.6% ± 0.94% and 1.89% ± 0.35%, respectively) (Fig. 2c). The membranes were relatively hydrophobic overall as shown in Fig. 2d. The water contact angle was smaller in the MMC-PLA/TBC membrane group (134.2° ± 1.22°) than in PLA/TBC membrane group (142.4° ± 5.6°) due to the hydrophilic MMC content.

We used a syringe pump method to study the release behavior of MMC in rabbit eyes and showed that there was continual release of MMC for 15 days (Fig. 3). The release rate of the stretched fibers was significantly slower ($p < 0.05$) than that of the original fibers, with an average daily release of 1.13 ± 0.32 μg, whereas the average rate of the original shape release was 4.70 ± 0.53 μg on the first day (Fig. 3a). According to Table S1, the first-order model provided the best fit for MMC release data. The n values for original and stretched fibers were 0.72 ± 0.05 and 0.77 ± 0.07, respectively. On day 7, the stretched fibers were heated to 43 °C and recovered to its original shape. After stretching, the fibrous membrane released 20% of MMC in the first 7 days. Thermal stimulation on day 7 accelerated drug release, leading to 69% cumulative release by day 15 (Fig. 3b).

Standard curve of MMC and the drug released from the fibers was validated using UV spectroscopy (Fig. S4a, b). There is a characteristic absorption peak at 365nm indicating that MMC can be effectively loaded and released from the PLA/TBC membranes [24]. Additionally, FTIR assessment showed that MMC did not affect the structure of PLA or react with it; the characteristic peaks of PLA are clearly visible for comparison in Fig. S4c. Therefore, MMC exhibits good compatibility with thermal-responsive PLA. Fig. S4d is the infrared spectrum of MMC. The

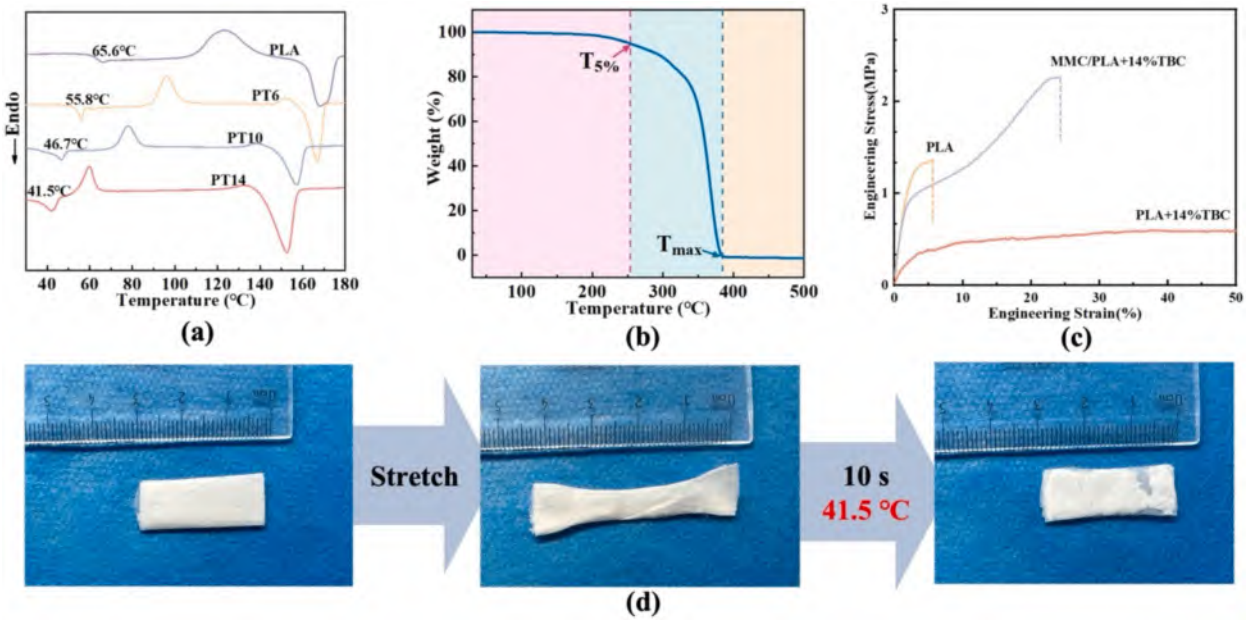

Fig. 1. Characterization and the properties of PLA/TBC. (a) Differential scanning calorimetry of different contents of TBC (PT = PLA/TBC). (b) TGA of PLA + 14% TBC membranes. (c) The stress-strain curves of PLA, PT14 and MMC/PT14 membranes. (d) Stretched membrane recovered within 10 s at 41.5 °C.

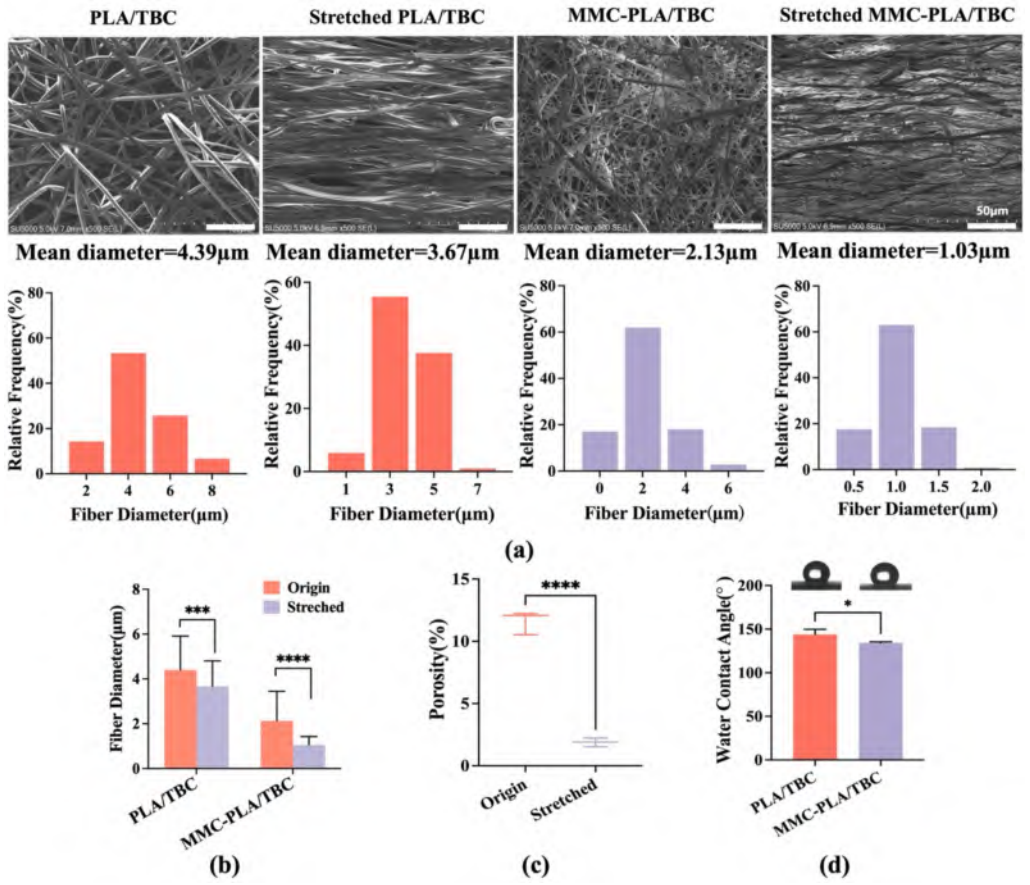

Fig. 2. Characterization of thermal-responsive PLA/TBC and MMC-PLA/TBC membranes. (a) SEM and diameter distribution of original and stretched fibers (PLA/TBC and MMC-PLA/TBC membranes); scale bar 50 μm. (b) Diameter of original and stretched fibers (PLA/TBC and MMC-PLA/TBC membranes). (c) Porosity of original and stretched MMC-PLA/TBC membranes. (d) Representative image and statistical result of water contact angle of PLA/TBC and MMC-PLA/TBC membranes in their original shape. *p < 0.05 as compared with the control.

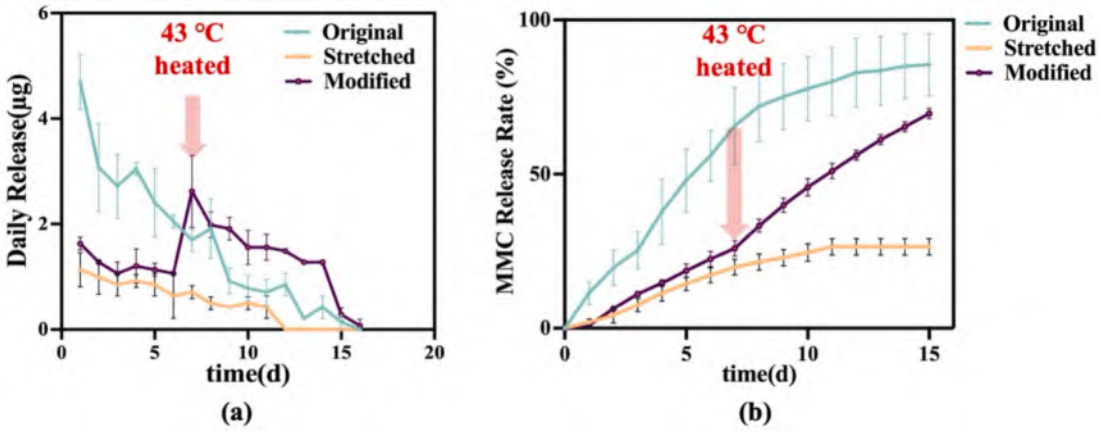

Fig. 3. Release profiles of MMC-PLA/TBC membranes. (a) Daily release and (b) MMC release rate of original MMC-PLA/TBC, stretched MMC-PLA/TBC, and modified MMC-PLA/TBC membranes (heated to 43 °C on day 7).

absence of MMC's characteristic peaks in the drug-loaded fibers could be due to the low drug loading or the dispersion of MMC within the polymer matrix.

3.3. Cytotoxicity and inhibitory effects of thermal-responsive fiber membranes

The expression of vimentin (+) and cytokeratin (−) was assessed to verify culture of the primary RTFs (Fig. S5). RTFs were cocultured with fibers in a medium containing fibers, and their viability was determined using live/dead staining (Fig. 4a). No obvious dead cells were observed in any of the groups. RTFs were also cultured on PLA/TBC membrane for 5 days. A limited number of cells adhered to the fiber surfaces and exhibited elongation along the fiber axis when seeded on the membranes, as demonstrated in Fig. 4b. Cell counting kit-8 (CCK-8) was applied to quantitatively assess the cytotoxicity of thermal-responsive

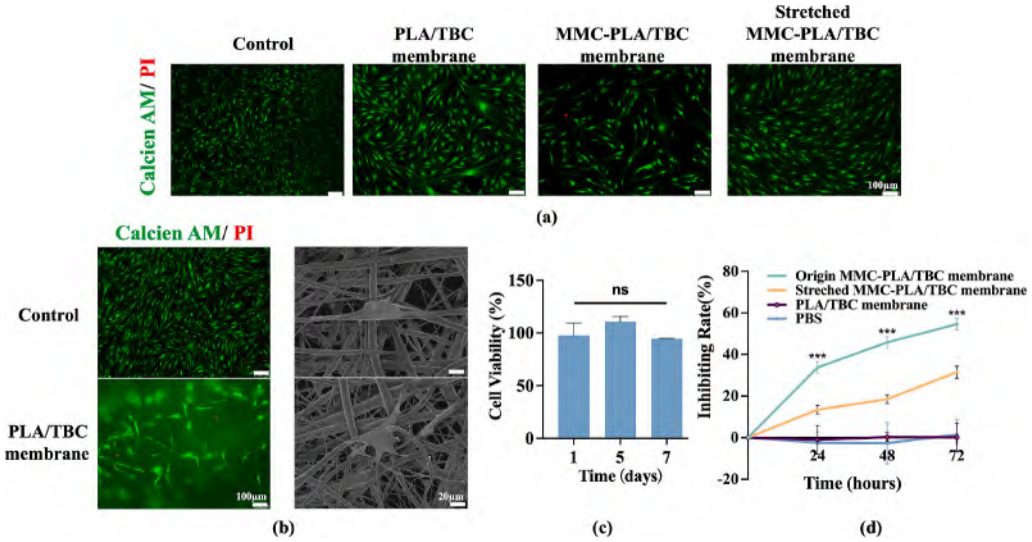

Fig. 4. Cytotoxicity and inhibitory effects of thermal-responsive PLA/TBC and MMC-PLA/TBC membranes. (a) Live/dead staining of the blank control, PLA/TBC membrane, MMC-PLA/TBC membrane, and stretched MMC-PLA/TBC membrane groups; scale bar 100 μm. (b) Live/dead staining of RTFs adhesion on PLA/TBC membrane; scale bar 100 μm; SEM images of RTFs adhesion on PLA/TBC membrane; scale bar 20 μm. (c) Cell viability after culture with PLA/TBC membranes on days 1, 5, and 7. (d) Cell growth inhibition rate after culture with the origin and stretched MMC-PLA/TBC membranes on days 1, 2, and 3. ***$p < 0.001$ as compared with the control.

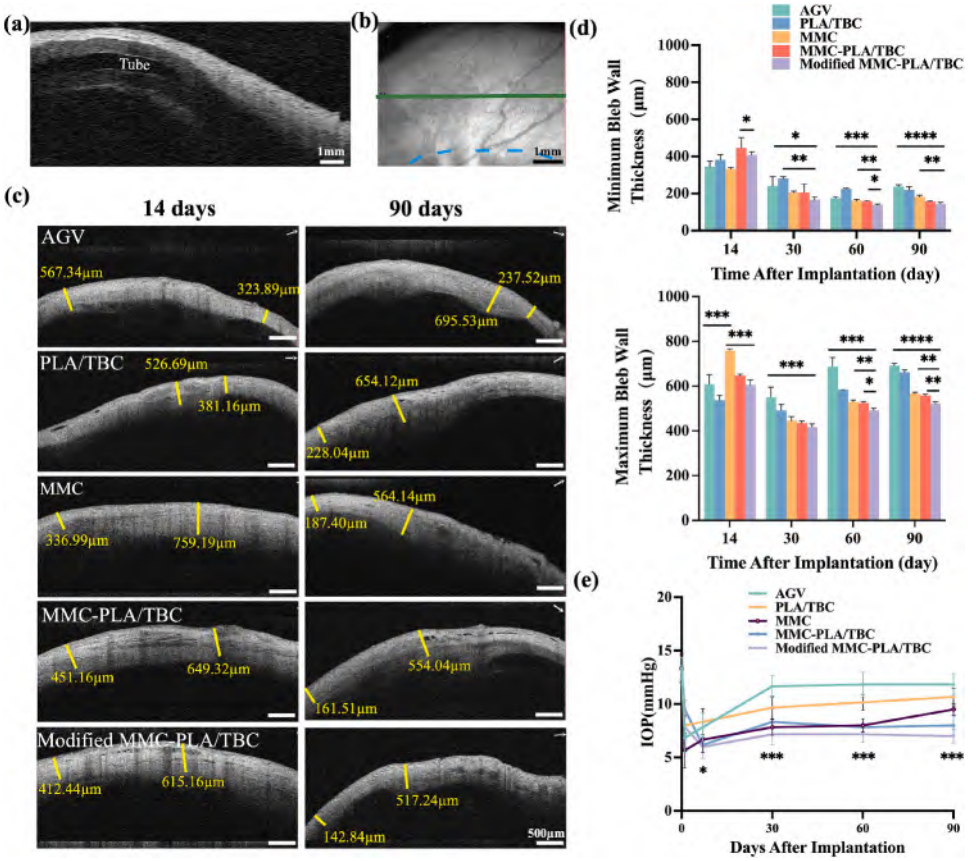

Fig. 5. Follow-up observations of eyes following surgery. (a) Representative image for a vertical scanning of AGV tube; scale bar 1 mm. (b) Scan position (green line), marker line (blue dotted line), and representative AGV tube images observed by AS-OCT on day 14; scale bar 1 mm. (c) Representative images and the wall thickness of bleb (yellow line) of AS-OCT 14 and 90 days postoperative for the AGV, PLA/TBC, MMC, MMC-PLA/TBC, and modified MMC-PLA/TBC groups; scale bar 500 μm. (d) Minimum and maximum of the bleb wall thickness for the AGV, PLA/TBC, MMC, MMC-PLA/TBC, and modified MMC-PLA/TBC groups, respectively. (e) IOP for the AGV, PLA/TBC, MMC, MMC-PLA/TBC, and modified MMC-PLA/TBC groups on days 1, 7, 30, 60, and 90 after implantation. *$p < 0.05$, ***$p < 0.001$ as modified MMC-PLA/TBC group compared with the control. (For interpretation of the references to color in this figure legend, the reader is referred to the web version of this article.)

polymers. On days 1, 5, and 7 of coculture with the PLA/TBC fibers, cell viability was close to 100% and showed no significant difference among days (Fig. 4c). MMC-PLA/TBC membranes inhibited RTFs growth and the inhibition rates of original and stretched MMC-PLA/TBC membranes both increased in time. On day 3, the inhibition rates of original and stretched MMC-PLA/TBC membranes on RTFs were 54.63% ± 2.89% and 31.48% ± 2.8%, respectively (Fig. 4d).

3.4. Follow-up observations of modified MMC-PLA/TBC membrane in vivo

Following implantation, the drainage tube remained clear as shown in Fig. 5a, and rabbits showed mild inflammatory signs like conjunctiva hyperemia and chemosis. On day 7, rabbit eyes treated with modified MMC-PLA/TBC were soaked in 43 °C saline for 30 s to recover from stretched shape and achieve faster MMC release. No eyes showed any sign of leakage, infection, or other serious complications (Figs. 5a, S6). The cornea remains transparent (Fig. S6b), indicating that 30 s of 43 °C stimulation was relatively safe for the ocular surface. Anterior segment optical coherence tomography (AS-OCT) was used to observe the thickness and condition of bleb wall on days 14, 30, 60, and 90, and representative images are presented in Fig. 5b. The thickness of bleb wall tested by AS-OCT could indicate the extent of bleb fibrosis *in vivo*. The thinner bleb wall thickness suggests less bleb fibrosis. Bleb walls were thicker at first due to the AGV implantations and MMC effect (Fig. 5c). Hyperemia and edema of the conjunctiva were more apparent during the first postoperative week, caused by the burst release of MMC [25]. Without MMC burst release, the modified group exhibited less edema (Fig. 5d) [26]. The minimum and maximum bleb wall thickness in the modified MMC-PLA/TBC group (144.70 ± 7.37 and 522.31 ± 8.33 μm, respectively) on day 90 were significantly thinner ($p < 0.05$) than those in the AGV group (237.30 ± 8.50 and 691.70 ± 10.41 μm, respectively), and MMC-PLA/TBC group (156.00 ± 5.29 and 557.70 ± 6.66 μm, respectively). The filtering bleb became progressively denser due to the accumulation of collagen, therefore, there is no significant increase of the bleb wall thickness between 60 and 90 days in the same group. Fibrosis of the filtering bleb leads to scarring and an increase in IOP, which is one of the main outcomes of AGV implanting for glaucoma patients. Therefore, lowering IOP could maintain the visual function of patients [27,28]. The pressure-sensitive unidirectional valve of AGV prevents complications caused by ocular hypotension [2]. Herein, the baseline IOP of rabbits was 13.4 ± 1.07 mmHg. The IOP of the AGV group increased and was maintained at a relatively high level during the following 30 postoperative days (Fig. 5e). The group treated with modified MMC-PLA/TBC kept a low level of IOP and reached 8.0 ± 0.89 mmHg 90 days postoperatively, which was significantly lower ($p < 0.05$) than that in AGV control group (11.83 ± 0.98 mmHg), MMC group (9.50 ± 0.55 mmHg), and MMC-PLA/TBC group (8.00 ± 0.89 mmHg). *In vivo* results demonstrate that the modified group had a lower IOP that effectively reduced scarring.

3.5. Toxicity and biocompatibility of modified MMC-PLA/TBC membrane

In addition to the *in vivo* experiments, this study was conducted from a histological perspective to verify the anti-fibrosis effect. There was no evidence of fiber residues after three months postoperatively, indicating that the fiber had fully degraded during this time. All treatment groups exhibited significantly greater fibrotic changes compared to normal conjunctival tissue. There was no significant evidence of inflammatory cells or necrotic tissues in any group as shown in Fig. 6. All groups revealed low toxicity and good biocompatibility.

3.6. Anti-fibrosis effect of modified MMC-PLA/TBC membrane

Fibrosis tissue, characterized by collagen deposition, stained blue with Masson's trichrome. Fibrosis tissue thickness was measured and compared in different regions (Fig. 7a). Previous research has shown that the foreign body reaction plays a primary role in fibrosis in GDD implant surgery [29]. The scar thickness of the modified MMC-PLA/TBC group except limbal side thickness was significantly thinner than that in the AGV group ($p < 0.0001$), and MMC-PLA/TBC group ($p < 0.01$) (Fig. 7b).

Immunohistochemical analysis (Fig. 8a, b) showed fewer α-SMA- and PCNA-positive cells in the modified MMC-PLA/TBC group ($p < 0.05$). α-SMA is expressed by myofibroblasts, and decreased expression of α-SMA indicates decreased differentiation of fibroblasts which leads to fibrosis [30]. Expression of PCNA is correlated with cell division; high expression of PCNA suggests the formation of a hypertrophic fibrosis tissue [31].

Interestingly, the fibrosis thickness of the PLA/TBC group was observed to be significantly thinner ($p < 0.05$) than that in the AGV group (Fig. 7b). To explain this result, we conducted immunofluorescence staining of Collagen type 1 (Col1) and Collagen type 3 (Col3). The ratio of Col1/Col3 in the AGV group (5.10 ± 1.31) was significantly increased ($p < 0.0001$) than in the PLA/TBC group and modified MMC-PLA/TBC group (1.44 ± 0.56 and 0.63 ± 0.18, respectively) (Fig. 9). Meanwhile, the ratio of Col1/Col3 in the modified MMC-PLA/TBC group was significantly lower ($p < 0.01$) than in the MMC-PLA/TBC group (1.20 ± 0.20).

4. Discussion

Ahmed Glaucoma Valve, as a foreign body in conjunctiva, could lead to formation of dense fibrous capsule [32]. According to a 5-year study, the surgical failure rate after AGV implantation increased over time [33]. The clinical application in glaucoma filtration surgery of MMC, which inhibit DNA synthesis, primarily depends on its potent anti-proliferative effects on subconjunctival fibroblasts, and induction of apoptosis in Tenon's capsule fibroblasts, thereby modulating post-operative wound healing processes [34]. Wound healing after glaucoma surgeries is a dynamic process. Fibroblasts migrate and massively proliferate postoperatively on days 5–14 (proliferative phase of scarring) [35,36]. Although MMC was released in vitro for 15 days, we believe

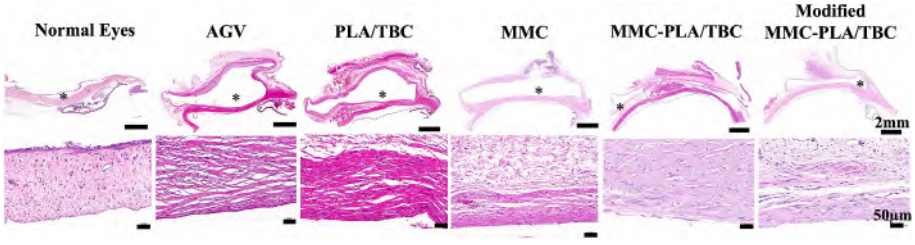

Fig. 6. H&E staining three months postoperatively demonstrated good biocompatibility of PLA/TBC, MMC, MMC-PLA/TBC, and modified MMC-PLA/TBC. (*: Filtration bleb area.)

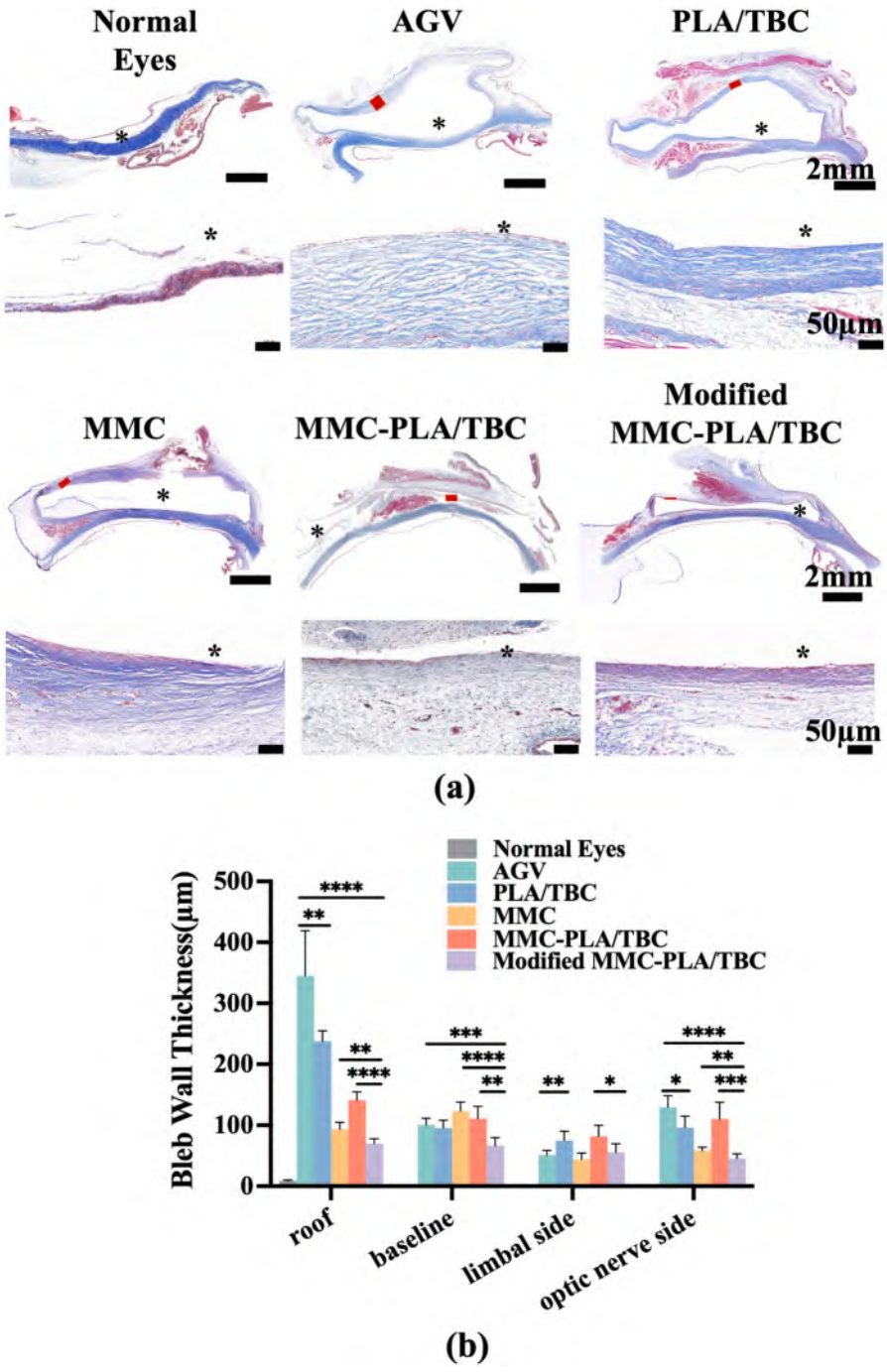

Fig. 7. Masson's trichrome staining of filtering blebs in the normal eyes, AGV, PLA/TBC, MMC, MMC-PLA/TBC, and modified MMC-PLA/TBC groups. (a) Representative micrograph of filtering bleb (*: Filtration bleb area). (b) Fibrosis tissue thickness of limbal side, optic nerve side, roof, and baseline bleb stained with Masson's trichrome in the normal eyes, AGV, PLA/TBC, MMC, MMC-PLA/TBC, and modified MMC-PLA/TBC groups. *$p < 0.05$ as compared with the control ($n = 6$).

that a release of 15 days could cover the critical period of fibrosis. We anticipate observing the long-term effect of dynamic release of MMC on bleb scarring. In this study, we observed the function of MMC-loaded thermal responsive fibers for a long term of 3 months and found modified MMC-PLA/TBC could remain low level of IOP and decrease fibrosis. MMC-induced fibroblast apoptosis is in a time- and concentration-dependent manner [37]. MMC treatment once would not cover the whole process of the proliferative phase when used once intraoperatively. Postoperative stimulation with saline at 43 °C could achieve the effect of subconjunctival injection and avoid serious side effects or drug toxicity caused by invasive manipulations and burst release. Therefore, we regulated PLA/TBC fiber membranes dynamically and achieved MMC controlled release *in vivo*, and effectively decreased the fibrosis in 3 months after AGV implantation.

Polyester-based materials were used for delivery of antiglaucoma medications [38,39]. PLA, as a polyester-based material, is biocompatible, biodegradable, and has an extensive range of biomedical applications in drug delivery [40]. The ocular surface temperature typically ranges from 33 °C to 35 °C [41], while the aqueous humor and conjunctival sac maintain a temperature of approximately 37 °C [42]. Overheating could cause cell death and other damage to the ocular surface [23]. Given this, the transition temperature of 41.5 °C and stimuli temperature of 43 °C for 30 seconds in our study were found to be safe for ocular tissues, consistent with previous studies on ocular

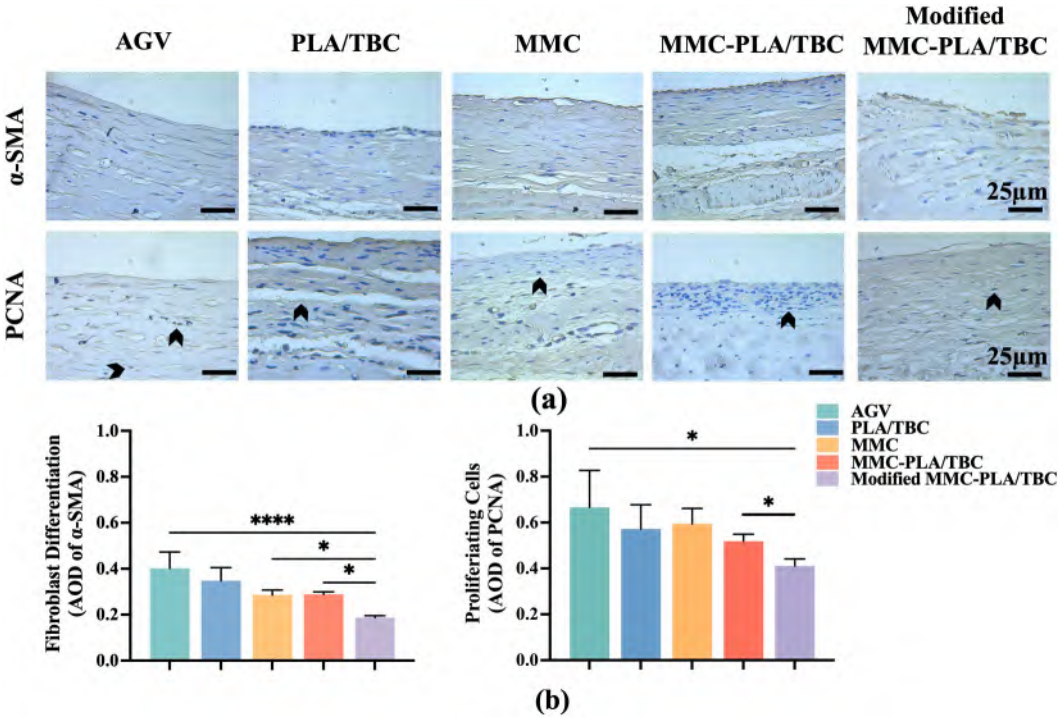

Fig. 8. Immunohistochemical examination three months postoperatively. (a) Representative graphs for the AGV, PLA/TBC, MMC, MMC-PLA/TBC, and modified MMC-PLA/TBC groups showing α-SMA-positive expression in cytoplasm and PCNA-positive expression in the nucleus (black arrows); scale bar 25 μm. (b) Average optical density of α-SMA- and PCNA-positive expression. *p < 0.05 as compared with the control (n = 6).

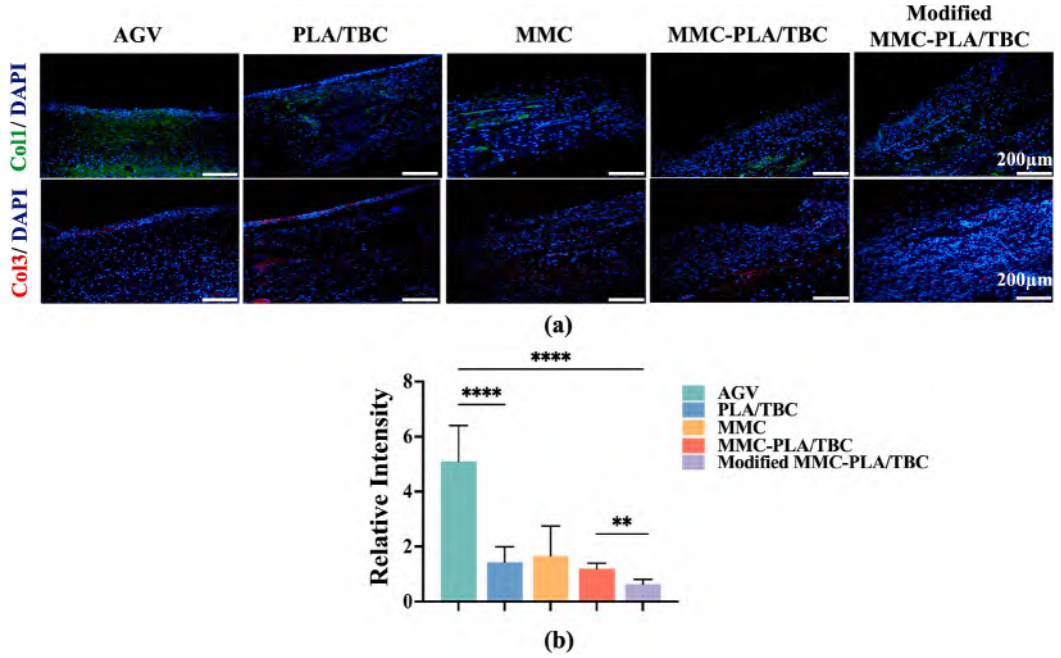

Fig. 9. Immunofluorescence staining of Col1 and Col3. (a) Graphs for the AGV, PLA/TBC, MMC, MMC-PLA/TBC, and modified MMC-PLA/TBC groups showing Col1 (green) and Col3 (red) expression; scale bar 200 μm. (b) Ratio of Col1/Col3 in AGV, PLA/TBC, MMC, MMC-PLA/TBC, and modified MMC-PLA/TBC groups. ****p < 0.0001 as compared with the control (n = 6). (For interpretation of the references to color in this figure legend, the reader is referred to the web version of this article.)

thermally responsive materials [43,44]. This good thermal-responsive property allows fibers achieve non-invasive deformation in vivo and reduce pain of patients.

Micro/nano-fibers have demonstrated considerable potential as drug delivery systems owing to their high porosity and high surface-to-volume ratio [45,46]. FTIR analysis confirmed that MMC did not affect the chemical structure of PLA. The characteristic peaks of PLA remained intact, suggesting no chemical interaction between MMC and PLA. Low drug content of fibers has been demonstrated to prolong release because the drug was encapsulated and dissolved in the fiber

[47]. Since the release exponent (n) values for all MMC formulations ranged from 0.43 to 0.85, the drug release mechanism can be classified as anomalous (non-Fickian) diffusion [48]. It can be inferred that PLA/TBC membranes effectively modulate MMC release kinetics, likely due to their controlled degradation and diffusion properties. Herein, MMC was mainly released by desorption and subsequent diffusion through water-filled pores. As results shown in Fig. 2a, the stretched fibers had aligned structures that led to lower burst release [49]. Moreover, the low porosity and the hydrophobicity of fibers was also found to inhibit drug release [50]. Tensile deformation arranges the fiber orientation to cause a decrease in the size of the pores between the fibers and in the overall porosity. The hydrophobic surface can reduce the rate of water absorption of the fibrous membrane, thereby slowing the rate of drug release [51]. This could explain the difference in drug release rate before and after fiber membrane deformation. The modified MMC-PLA/TBC membrane in this study showed an initial slow release followed by a fast release pattern and achieved controlled MMC release.

Cytotoxicity tests showed that PLA/TBC membranes had favorable biological applicability. Low concentrations of MMC are known to inhibit cell proliferation with low cytotoxicity [52]. Proliferation and differentiation of Tenon's fibroblasts is one of the main reasons for scarring after glaucoma surgery [53]. Fibroblasts' proliferation reaches the peak one week postoperatively [54], shape recovering of MMC-PLA/TBC membranes could inhibit RTFs effectively. Consistent with drug release characteristics, the inhibition of cell proliferation in the group treated with stretched MMC-PLA/TBC membranes was less than that in the group treated with original unstretched membranes. The amount of MMC released from both original and stretched micro/nano-fibers was proofed to be sufficient for inhibiting fibroblasts proliferation according to previous study [10]. In addition, RTFs adhesion could be prevented on hydrophobic fiber membranes [55]. Based on the *in vitro* experiments, drug-loaded fiber membranes offer favorable biological safety and could effectively control cell proliferation by changing fibers' shape.

The possible mechanisms of the modified MMC-PLA/TBC micro/nanofibers reducing fibrosis were as follows. First, MMC-controlled release dynamically inhibited the proliferation and adhesion of fibroblasts during the entire proliferative phase of scarring. The reduced fibroblast population consequently differentiated into fewer myofibroblasts with an overall decreased expression level of collagen, α-SMA and PCNA and a thinner bleb wall. Second, the fiber-coated AGV increased the MMC application area, which guaranteed enough fixed space for MMC to function, as previously shown that could decrease fibrosis of bleb wall [9]. Third, the soft fibers relieved mechanical overloading conditions and provided a wound healing environment without excessive fibrosis. During scar formation, Col3 is first deposited in the ECM and then gradually replaced by Col1 [56]. The increase of Col1/Col3 ratio indicates the excessive fibrosis. Zhou et al. found that mechanical overloading could increase the ratio of Col1/Col3 [57]. A flexible, soft fibrous membrane covered-AGV may relieve the mechanical press of silicone-made AGV. Meanwhile, the ECM-like structure of micro/nanofibrous membranes could lead to non-scarring healing [58,59]. In this condition, the wound tended to recover without excessive fibrosis. Less differentiation of fibroblasts and MMC-controlled release together reduced the scarring associated with AGV implantation.

This study has some limitations. The release time of MMC was shorter than that in previous studies [55,60], and a core–shell structure of fibers may provide longer drug release time. Furthermore, while this study focused on the safety of 43 °C for ocular surface and filtering bleb, further investigation is needed to determine how thermal exposure influences bleb fibrosis. Additionally, the use of normal rabbit models may not fully replicate the conditions seen in glaucomatous patients, where factors like high intraocular pressure and cytokine levels such as vascular endothelial growth factor [61] and transforming growth factor-beta [62] play a more significant role in fibrosis development. Therefore, rabbit models with stable high IOP need to be investigated in further research.

5. Conclusions

This study introduced a system featuring dynamic regulation of thermal-responsive fibers for controlled drug release in ophthalmology. The thermal-responsive fiber showed considerable potential in dynamic controlled drug release applications. Thermal-responsive MMC-PLA/TBC membranes and use of the transition temperature were shown to be biologically safe. The release of MMC could be dynamically regulated to prevent burst release and significantly inhibit RTF proliferation. The noninvasive MMC release regulation was achieved by heating simulation on the ocular surface to effectively decrease fibrosis. Therefore, the thermal-responsive MMC-loaded PLA/TBC fiber membrane has potential clinical value for glaucoma surgery and translational potential for non-invasive drug delivery.

CRediT authorship contribution statement

Jingyi Ma: Writing – original draft, Validation, Methodology, Investigation, Data curation. **Lu Wang:** Writing – original draft, Methodology, Investigation, Data curation. **Aimeng Dong:** Supervision, Project administration, Methodology. **Shiqi Zhang:** Supervision, Project administration, Investigation. **Tao Guo:** Investigation, Data curation. **Yiling Han:** Investigation, Data curation. **Menglu Jiang:** Investigation, Data curation. **Pan Fan:** Validation, Investigation. **Wulian Song:** Validation, Project administration, Funding acquisition. **Fenghua Zhang:** Writing – review & editing, Project administration, Funding acquisition. **Jinsong Leng:** Writing – review & editing, Conceptualization. **Huiping Yuan:** Writing – review & editing, Funding acquisition, Conceptualization.

Statement of animal rights

All animal study protocols were approved by the Animal Ethics Committee of the Second Affiliated Hospital of Harbin Medical University (SYDW2020-072).

Declaration of competing interest

The authors declare no conflict of interest.

Acknowledgments

This work was supported by the National Natural Science Foundation of China (Grant No. 81870654, 82070956, 82000889, and 11802075), and Applied Technology Research and Development Program of Heilongjiang Provincial Science and Technology Department (GA20C008). AGV was generously provided by Beijing Hebang Site Technology Development Co., Ltd.

Appendix A. Supplementary data

Supplementary data to this article can be found online at https://doi.org/10.1016/j.bioadv.2025.214359.

Data availability

The datasets used and analyzed during the current study are available from the corresponding author on reasonable request.

References

[1] J.B. Jonas, T. Aung, R.R. Bourne, A.M. Bron, R. Ritch, S. Panda-Jonas, Glaucoma, Lancet 390 (2017) 2183–2193, https://doi.org/10.1016/S0140-6736(17)31469-1.
[2] I. Riva, G. Roberti, F. Oddone, A.G. Konstas, L. Quaranta, Ahmed glaucoma valve implant: surgical technique and complications, OPTH 11 (2017) 357–367, https://doi.org/10.2147/OPTH.S104220.

[3] M. Zada, U. Pattamatta, A. White, Modulation of fibroblasts in conjunctival wound healing, Ophthalmology 125 (2018) 179–192, https://doi.org/10.1016/j.ophtha.2017.08.028.

[4] S.K. Law, A modified technique of Ahmed glaucoma valve implantation with adjunctive use of antifibrotic agents, Am. J. Ophthalmol. 146 (2008) 156–158, https://doi.org/10.1016/j.ajo.2008.05.003.

[5] V.H.X. Foo, H.M. Htoon, D.S. Welsbie, S.A. Perera, Aqueous shunts with mitomycin C versus aqueous shunts alone for glaucoma, Cochrane Database Syst. Rev. (2019) CD011875, https://doi.org/10.1002/14651858.CD011875.pub2.

[6] C.I. Perez, S. Verdaguer, D. Khaliliyeh, E.A. Maul, Y. Ou, Y. Han, Subconjunctival injections of mitomycin C are associated with a lower incidence of hypertensive phase in eyes with Ahmed glaucoma valve, Ophthalmology Glaucoma 4 (2021) 322–329, https://doi.org/10.1016/j.ogla.2020.10.004.

[7] F.F. Reichel, V. Guggenberger, H. Faber, J. Neubauer, B. Voykov, Results of XEN45 gel stent implantation in the treatment of primary open-angle glaucoma using 5, 10 or 20 μg mitomycin C: a pilot study, J. Ophthalmol. 2024 (2024) 3895054, https://doi.org/10.1155/2024/3895054.

[8] J.L. Do, B.Y. Xu, B. Wong, A. Camp, P. Ngai, C. Long, et al., A randomized controlled trial comparing subconjunctival injection to direct scleral application of Mitomycin C in trabeculectomy, Am. J. Ophthalmol. 220 (2020) 45–52, https://doi.org/10.1016/j.ajo.2020.07.002.

[9] M. Zhou, W. Wang, W. Huang, X. Zhang, Use of Mitomycin C to reduce the incidence of encapsulated cysts following ahmed glaucoma valve implantation in refractory glaucoma patients: a new technique, BMC Ophthalmol. 14 (2014) 107, https://doi.org/10.1186/1471-2415-14-107.

[10] A. Dong, L. Han, Z. Shao, P. Fan, X. Zhou, H. Yuan, Glaucoma drainage device coated with mitomycin C loaded opal shale microparticles to inhibit bleb fibrosis, ACS Appl. Mater. Interfaces 11 (2019) 10244–10253, https://doi.org/10.1021/acsami.8b18551.

[11] E.D. Schoenberg, D.A. Blake, F.B. Swann, A.W. Parlin, D. Zurakowski, C.E. Margo, et al., Effect of two novel sustained-release drug delivery systems on bleb fibrosis: an in vivo glaucoma drainage device study in a rabbit model, Transl. Vis. Sci. Technol. 4 (2015) 4, https://doi.org/10.1167/tvst.4.3.4.

[12] L. Chang, J.G. Crowston, M.F. Cordeiro, A.N. Akbar, P.T. Khaw, The role of the immune system in conjunctival wound healing after glaucoma surgery, Surv. Ophthalmol. 45 (2000) 49–68, https://doi.org/10.1016/S0039-6257(00)00135-1.

[13] Y. Xia, Y. He, F. Zhang, Y. Liu, J. Leng, A review of shape memory polymers and composites: mechanisms, materials, and applications, Adv. Mater. 33 (2021) 2000713, https://doi.org/10.1002/adma.202000713.

[14] C. Chen, J. Wang, Z. Xu, N. Chen, F. Wang, Highly stretchable, self-healable and adhesive, thermal responsive conductive hydrogel loading nanocellulose complex for a flexible sensor, Int. J. Biol. Macromol. 247 (2023) 125595, https://doi.org/10.1016/j.ijbiomac.2023.125595.

[15] D.D. Nguyen, L.-J. Luo, J.-Y. Lai, Dendritic effects of injectable biodegradable thermogels on pharmacotherapy of inflammatory glaucoma-associated degradation of extracellular matrix, Adv. Healthc. Mater. 8 (2019) 1900702, https://doi.org/10.1002/adhm.201900702.

[16] L.-J. Luo, D.D. Nguyen, J.-Y. Lai, Benzoic acid derivative-modified chitosan-g-poly (N-isopropylacrylamide): methoxylation effects and pharmacological treatments of glaucoma-related neurodegeneration, J. Control. Release 317 (2020) 246–258, https://doi.org/10.1016/j.jconrel.2019.11.038.

[17] D.D. Nguyen, L.-J. Luo, S.J. Lue, J.-Y. Lai, The role of aromatic ring number in phenolic compound-conjugated chitosan injectables for sustained therapeutic antiglaucoma efficacy, Carbohydr. Polym. 231 (2020) 115770, https://doi.org/10.1016/j.carbpol.2019.115770.

[18] M. Bao, X. Lou, Q. Zhou, W. Dong, H. Yuan, Y. Zhang, Electrospun biomimetic fibrous scaffold from shape memory polymer of PDLLA-co-TMC for bone tissue engineering, ACS Appl. Mater. Interfaces 6 (2014) 2611–2621, https://doi.org/10.1021/am405101k.

[19] L. Tan, J. Hu, H. Huang, J. Han, H. Hu, Study of multi-functional electrospun composite nanofibrous mats for smart wound healing, Int. J. Biol. Macromol. 79 (2015) 469–476, https://doi.org/10.1016/j.ijbiomac.2015.05.014.

[20] C. Lin, L. Liu, Y. Liu, J. Leng, 4D printing of bioinspired absorbable left atrial appendage occluders: a proof-of-concept study, ACS Appl. Mater. Interfaces 13 (2021) 12668–12678, https://doi.org/10.1021/acsami.0c17192.

[21] M. Zare, P. Davoodi, S. Ramakrishna, Electrospun shape memory polymer micro-/nanofibers and tailoring their roles for biomedical applications, Nanomaterials (Basel) 11 (2021) 933, https://doi.org/10.3390/nano11040933.

[22] D.D. Nguyen, J.-Y. Lai, Advancing the stimuli response of polymer-based drug delivery systems for ocular disease treatment, Polym. Chem. 11 (2020) 6988–7008, https://doi.org/10.1039/D0PY00919A.

[23] X. Zheng, L. Xin, Y. Luo, H. Yang, X. Ye, Z. Mao, et al., Near-infrared-triggered dynamic surface topography for sequential modulation of macrophage phenotypes, ACS Appl. Mater. Interfaces 11 (2019) 43689–43697, https://doi.org/10.1021/acsami.9b14808.

[24] L. Qi, C. Liu, Y. Zhang, Z. Zhang, H. Duan, H. Zhao, et al., Development of mitomycin C-loaded nanoparticles prepared using the micellar assembly driven by the combined effect of hydrogen bonding and π–π stacking and its therapeutic application in bladder cancer, Pharmaceutics 13 (2021) 1776, https://doi.org/10.3390/pharmaceutics13111776.

[25] M. Ibarz Barberá, L. Morales Fernández, P. Tañá Rivero, R. Gómez de Liaño, M. A. Teus, Anterior-segment optical coherence tomography of filtering blebs in the early postoperative period of ab externo SIBS microshunt implantation with mitomycin C: morphological analysis and correlation with intraocular pressure reduction, Acta Ophthalmol. (2021) aos.14863, https://doi.org/10.1111/aos.14863.

[26] X. Huang, C.S. Brazel, On the importance and mechanisms of burst release in matrix-controlled drug delivery systems, J. Control. Release 73 (2001) 121–136, https://doi.org/10.1016/s0168-3659(01)00248-6.

[27] N.E. Tan, S.X. Chen, A.H. Fang, N.M. Radcliffe, Outcomes of sutureless ahmed glaucoma valve surgery: a retrospective study, Ophthalmol Therapy 11 (2022) 2083–2100, https://doi.org/10.1007/s40123-022-00565-0.

[28] L. Trigler, A.D. Proia, S.F. Freedman, Fibrovascular ingrowth as a cause of Ahmed glaucoma valve failure in children, Am. J. Ophthalmol. 141 (2006) 388–389, https://doi.org/10.1016/j.ajo.2005.08.033.

[29] K.I. Jung, S.-B. Lee, J.H. Kim, C.K. Park, Foreign body reaction in glaucoma drainage implant surgery, Invest. Ophthalmol. Vis. Sci. 54 (2013) 3957–3964, https://doi.org/10.1167/iovs.12-11310.

[30] D. Dolivo, P. Weathers, T. Dominko, Artemisinin and artemisinin derivatives as anti-fibrotic therapeutics, Acta Pharm. Sin. B 11 (2021) 322–339, https://doi.org/10.1016/j.apsb.2020.09.001.

[31] J.-C. Zhao, B.-R. Zhang, L. Hong, K. Shi, W.-W. Wu, J.-A. Yu, Extracorporeal shock wave therapy with low-energy flux density inhibits hypertrophic scar formation in an animal model, Int. J. Mol. Med. 41 (2018) 1931–1938, https://doi.org/10.3892/ijmm.2018.3434.

[32] K.I. Jung, C.K. Park, Pirfenidone inhibits fibrosis in foreign body reaction after glaucoma drainage device implantation, Drug Des. Devel. Ther. 10 (2016) 1477–1488, https://doi.org/10.2147/DDDT.S99957.

[33] P.G. Christakis, J.W. Kalenak, J.C. Tsai, D. Zurakowski, J.A. Kammer, P. J. Harasymowycz, et al., The Ahmed Versus Baerveldt Study: five-year treatment outcomes, Ophthalmology 123 (2016) 2093–2102, https://doi.org/10.1016/j.ophtha.2016.06.035.

[34] S. Van de Velde, T. Van Bergen, E. Van dewalle, L. Moons, I. Stalmans, Chapter 16 - modulation of wound healing in glaucoma surgery, in: G. Bagetta, C. Nucci (Eds.), Progress in Brain Research vol. 221, Elsevier, 2015, pp. 319–340, https://doi.org/10.1016/bs.pbr.2015.05.002.

[35] N.J. Collignon, Wound healing after glaucoma surgery: how to manage it? Bull. Soc. Belge Ophtalmol. (2005) 55–59.

[36] P.J. Lama, R.D. Fechtner, Antifibrotics and wound healing in glaucoma surgery, Surv. Ophthalmol. 48 (2003) 314–346, https://doi.org/10.1016/S0039-6257(03)00038-9.

[37] J.G. Crowston, A.N. Akbar, P.H. Constable, N.L. Occleston, J.T. Daniels, P.T. Khaw, Antimetabolite-induced apoptosis in Tenon's capsule fibroblasts, Invest. Ophthalmol. Vis. Sci. 39 (1998) 449–454.

[38] D.D. Nguyen, L.-J. Luo, J.-Y. Lai, Effects of shell thickness of hollow poly(lactic acid) nanoparticles on sustained drug delivery for pharmacological treatment of glaucoma, Acta Biomater. 111 (2020) 302–315, https://doi.org/10.1016/j.actbio.2020.04.055.

[39] A. Josyula, A. Mozzer, J. Szeto, Y. Ha, N. Richmond, S.W. Chung, et al., Nanofiber-based glaucoma drainage implant improves surgical outcomes by modulating fibroblast behavior, Bioeng Transl Med 8 (2023) e10487, https://doi.org/10.1002/btm2.10487.

[40] B. Tyler, D. Gullotti, A. Mangraviti, T. Utsuki, H. Brem, Polylactic acid (PLA) controlled delivery carriers for biomedical applications, Adv. Drug Deliv. Rev. 107 (2016) 163–175, https://doi.org/10.1016/j.addr.2016.06.018.

[41] I. Koçak, S. Orgül, J. Flammer, Variability in the measurement of corneal temperature using a noncontact infrared thermometer, Ophthalmologica 213 (1999) 345–349, https://doi.org/10.1159/000027452.

[42] W. Wang, X. Qian, H. Song, M. Zhang, Z. Liu, Fluid and structure coupling analysis of the interaction between aqueous humor and iris, Biomed. Eng. Online 15 (2016) 133, https://doi.org/10.1186/s12938-016-0261-3.

[43] A.I. Rem, J.A. Oosterhuis, H.G. Journée-de Korver, T.J. van den Berg, J.E. Keunen, Temperature dependence of thermal damage to the sclera: exploring the heat tolerance of the sclera for transscleral thermotherapy, Exp. Eye Res. 72 (2001) 153–162, https://doi.org/10.1006/exer.2000.0939.

[44] J.G. Bollemeijer, J.J. Lagendijk, J.A. van Best, A.A. de Leeuw, J.L. van Delft, D. de Wolff-Rouendaal, et al., Effects of microwave-induced hyperthermia on the anterior segment of healthy rabbit eyes, Graefes Arch. Clin. Exp. Ophthalmol. 227 (1989) 271–276, https://doi.org/10.1007/BF02172761.

[45] C.R. Gough, X. Hu, Air-spun silk-based micro-/nanofibers and thin films for drug delivery, Int. J. Mol. Sci. 22 (2021) 9588, https://doi.org/10.3390/ijms22179588.

[46] M. Kamaraj, N. Moghimi, A. McCarthy, J. Chen, S. Cao, A.R. Chethikkattuveli Salih, et al., Granular porous nanofibrous microspheres enhance cellular infiltration for diabetic wound healing, ACS Nano (2024), https://doi.org/10.1021/acsnano.4c10044.

[47] M.V. Natu, H.C. de Sousa, M.H. Gil, Effects of drug solubility, state and loading on controlled release in bicomponent electrospun fibers, Int. J. Pharm. 397 (2010) 50–58, https://doi.org/10.1016/j.ijpharm.2010.06.045.

[48] L. Ahmed, R. Atif, T. Eldeen, I. Yahya, A. Omara, M. Eltayeb, Study the using of nanoparticles as drug delivery system based on mathematical models for controlled release 8 (2019) 52–56.

[49] M. Eslamian, M. Khorrami, N. Yi, S. Majd, M.R. Abidian, Electrospinning of highly aligned fibers for drug delivery applications, J. Mater. Chem. B 7 (2019) 224, https://doi.org/10.1039/C8TB01258J.

[50] A. Rahma, M.M. Munir, Prasetyo A. Khairurrijal, V. Suendo, H. Rachmawati, Intermolecular interactions and the release pattern of electrospun curcumin-polyvinyl(pyrrolidone) fiber, Biol. Pharm. Bull. 39 (2016) 163–173, https://doi.org/10.1248/bpb.b15-00391.

[51] T.N. Hiew, D.L.H. Tan, Y.L. Tiang, P.W.S. Heng, Understanding the release performance of pellets with hydrophobic inclusions in sustained-release coating, Int. J. Pharm. 557 (2019) 229–237, https://doi.org/10.1016/j.ijpharm.2018.12.061.

[52] R. Gupta, B.W. Yarnall, E.A. Giuliano, J.R. Kanwar, D.G. Buss, R.R. Mohan, Mitomycin C: a promising agent for the treatment of canine corneal scarring, Vet. Ophthalmol. 14 (2011) 304–312, https://doi.org/10.1111/j.1463-5224.2011.00877.x.
[53] J.E.J. Wolters, R.J.S. van Mechelen, R. Al Majidi, L. Pinchuk, C.A.B. Webers, H.J. M. Beckers, et al., History, presence, and future of mitomycin C in glaucoma filtration surgery, Curr. Opin. Ophthalmol. 32 (2021) 148–159, https://doi.org/10.1097/ICU.0000000000000729.
[54] A. Lockwood, S. Brocchini, P.T. Khaw, New developments in the pharmacological modulation of wound healing after glaucoma filtration surgery, Curr. Opin. Pharmacol. 13 (2013) 65–71, https://doi.org/10.1016/j.coph.2012.10.008.
[55] X. Zhao, S. Jiang, S. Liu, S. Chen, Z.Y.W. Lin, G. Pan, et al., Optimization of intrinsic and extrinsic tendon healing through controllable water-soluble mitomycin-C release from electrospun fibers by mediating adhesion-related gene expression, Biomaterials 61 (2015) 61–74, https://doi.org/10.1016/j.biomaterials.2015.05.012.
[56] C. Profyris, C. Tziotzios, Vale I. Do, Cutaneous scarring: pathophysiology, molecular mechanisms, and scar reduction therapeutics part I. The molecular basis of scar formation, J. Am. Acad. Dermatol. 66 (2012) 1–10, https://doi.org/10.1016/j.jaad.2011.05.055 (quiz 11–2).
[57] Y. Zhou, Y. Zhao, H. Du, Y. Suo, H. Chen, H. Li, et al., Downregulation of CFTR is involved in the formation of hypertrophic scars, Biomed. Res. Int. 2020 (2020) 9526289, https://doi.org/10.1155/2020/9526289.
[58] S. Ahn, C.O. Chantre, A.R. Gannon, J.U. Lind, P.H. Campbell, T. Grevesse, et al., Soy protein/cellulose nanofiber scaffolds mimicking skin extracellular matrix for enhanced wound healing, Adv. Healthc. Mater. 7 (2018) e1701175, https://doi.org/10.1002/adhm.201701175.
[59] A.D. Juncos Bombin, N.J. Dunne, H.O. McCarthy, Electrospinning of natural polymers for the production of nanofibres for wound healing applications, Mater. Sci. Eng. C Mater. Biol. Appl. 114 (2020) 110994, https://doi.org/10.1016/j.msec.2020.110994.
[60] F. Zhang, K. Liu, Z. Pan, M. Cao, D. Zhou, H. Liu, et al., Effects of rosiglitazone/PHBV drug delivery system on postoperative fibrosis in rabbit glaucoma filtration surgery model, Drug Deliv. 26 (2019) 812–819, https://doi.org/10.1080/10717544.2019.1648590.
[61] D.-N. Hu, R. Ritch, J. Liebmann, Y. Liu, B. Cheng, M.S. Hu, Vascular endothelial growth factor is increased in aqueous humor of glaucomatous eyes, J. Glaucoma 11 (2002) 406–410, https://doi.org/10.1097/00061198-200210000-00006.
[62] R.C. Tripathi, J. Li, W.F. Chan, B.J. Tripathi, Aqueous humor in glaucomatous eyes contains an increased level of TGF-beta 2, Exp. Eye Res. 59 (1994) 723–727, https://doi.org/10.1006/exer.1994.1158.